ELSEVIER

Journal of Molecular Catalysis A: Chemical 272 (2007) 11–19

MOLECULAR CATALYSIS A: CHEMICAL

www.elsevier.com/locate/molcata

Accelerated photodegradation (minute range) of the commercial azo-dye Orange II mediated by Co_3O_4/Raschig rings in the presence of oxone

Yu Zhiyong [a,b], M. Bensimon [c], D. Laub [d], L. Kiwi-Minsker [a], W. Jardim [e,f,*], E. Mielczarski [e,f], J. Mielczarski [e,f], J. Kiwi [a,*]

[a] *Laboratory of Chemical Reaction Engineering LGRC, Station 6, Swiss Federal Institute of Technology (EPFL), Lausanne 1015, Switzerland*
[b] *Department of Chemistry, Renmin University of China, Beijing 100872, China*
[c] *EPFL-ENAC-Geolep, Station 18, Brazil*
[d] *EPFL-SB-CIME, Station 18, Brazil*
[e] *Institute of Chemistry, UNICAMP, State University of Campinas, Brazil*
[f] *NPL/CNRS, UMR 7569 LEM, 15 av du Charmois, 54501 Vandoeuvre les Nancy, France*

Received 23 November 2006; accepted 2 March 2007
Available online 15 March 2007

Abstract

The accelerated discoloration of Orange II by an innovative Co_3O_4/Raschig ring photocatalyst (from now on Co_3O_4/RR) is feasible and proceeds to completion using oxone as an oxidant within the surprisingly short time of ~5 min. The preparation of Co_3O_4 small clusters (2–10 nm in size) on RR is reported. The discoloration/mineralization of the azo-dye Orange II was carried out in a concentric coaxial photo-reactor and was a function of the Orange II and oxone concentrations, the solution pH and the recirculation rate. At bio-compatible pH-values, the concentration of Co-ions in solution after photocatalysis (15 min) was found to be between 0.5 and 2 ppm, within the limits allowed for treated waters. The generation of peroxide was observed as long as Orange II was still available in solution.

By elemental analysis (EA), the amount of Co of the Raschig rings was determined to be ~65% (w/w) before and after the photocatalysis. This confirms the stability observed during long-term operation of the Co_3O_4/RR catalyst. The sizes of the Co_3O_4 clusters on the RR surface were determined by transmission electron spectroscopy (TEM). A non-uniform distribution of Co_3O_4 particles on RR with sizes between 2 and 10 nm was found. The presence of Co-clusters on the RR-surface was confirmed by electron dispersive spectroscopy (EDS) showing 12.6% surface Co-enrichment before the photocatalysis and 18.8% surface enrichment after the photocatalysis. By confocal microscopy the irregularly thick shaped Co_3O_4 on the Raschig rings was analyzed. The most striking observation is very large shift of Co2p3/2 line from 779.6 eV at time zero to 782.2 eV within 10 min after due to the photocatalysis taking place. This indicates a strong reduction of electron density on the cobalt atoms of Co_3O_4/RR and providing the evidence for the strong oxidation properties of this catalyst.

Keywords: Discoloration/mineralization; Orange II; Oxone; Co_3O_4/Raschig rings; Photo-reactor

1. Introduction

Photocatalytic degradation has attracted increasing attention during the last decade as a promising technology for the removal of non-biodegradable and toxic contaminants from wastewater [1,2]. However, the practical application of photocatalysis to destroy recalcitrant pollutants by stable catalysts has not been fully attained. This is due to the poor kinetic performance of the available photocatalysts to treat economically industrial waste waters [3,4]. Long treatment times in waste water remediation applying photocatalysis involve a high amount of expensive UV-photons. This constitutes a high cost factor compared to the cost of the oxidation reagent required in processes belonging to the field of Advanced Oxidation Technologies (AOT's) [5].

Oxone as an oxidant decomposed by metal-ions or oxides to degrade pollutants has revealed effective, but it presents the drawback of homogeneous systems [1–5]. The practical limitation for the use of heterogeneous photocatalysts in powder form is the separation of the heterogeneous catalyst at the end of the treatment. Thus, the catalyst immobilization is a necessary step

* Corresponding authors. Tel.: +41 21 8017536; fax: +41 21 6934111.
E-mail address: john.kiwi@epfl.ch (J. Kiwi).

1381-1169/$ – see front matter © 2007 Elsevier B.V. All rights reserved.
doi:10.1016/j.molcata.2007.03.023

to avoid the costly end-of-pipe separation step [6]. In our laboratory, the immobilization of TiO_2 on Raschig rings (RR) has been recently the subject of some recent studies concerning the degradation pollutants under light irradiation [7–9]. As a natural continuation of these studies, the present work addresses the fixation of Co_3O_4 on Raschig rings to produce a catalyst that would accelerate oxone decomposition. The Orange II is a textile non-biodegradable commercial dye and has been selected as the probe organic compound to test the photodiscoloration and mineralization kinetics by the oxone-Co_3O_4/RR system.

The fixation of Co_3O_4 on Raschig rings was designed in such a way that small clusters of Co_3O_4 could be suitably produced and permanently fixed on the RR. This support was selected since: (a) it resists the attack of the highly oxidative radicals generated by the oxone decomposition catalyzed by Mn^{2+} or Cu^{2+} [10,11], (b) it also resists he decomposition of oxone recently reported by Co^{2+}-ions [12,13] and (c) provides a large surface area in the reactor to induce accelerated Orange II decomposition. The short photodiscoloration times attained in the minute range are impressive compared with times needed by the TiO_2/RR photocatalyst to degrade organic compounds under similar experimental conditions irradiation [7–9]. The experimental evidence for the accelerated kinetic performance observed is provided by XPS spectroscopy by identifying unambiguously the strong oxidation properties of the Co_3O_4.

2. Experimental

2.1. Reagents and materials

Orange II, NaOH, acids, H_2O_2, $CoSO_4{\cdot}7H_2O$ were Fluka p.a. reagents (Buchs, Switzerland) and used without further purification. Oxone is potassium peroxy-monosulfate $2KSO_5{\cdot}KHSO_4{\cdot}K_2SO_4$ [CAS-RN 10058-23-8] and was obtained from Aldrich Chemicals (Buchs, Switzerland, catalogue No. 22803-6). Tri-distilled water was used throughout the experiments. The cylindrical Raschig rings from Carrouge Glass-works (VD, Switzerland) had a length of 4 mm, an external diameter of 4 mm, and an internal diameter of 3 mm. The soda lime of the glass consisted of: 70% SiO_2, 10% (Na_2O, CaO, MgO, K_2O), and 5% (Fe_2O_3, Al_2O_3 and a few other trivalent oxides and anionic impurities in trace amounts).

2.2. Fixation of Co_3O_4 and Fe_2O_3 on Raschig rings

The Raschig rings were etched with dilute HF for 10 h, washed thoroughly with tri-distilled water and dried at 110 °C. The colloid used to deposit the Co_3O_4 on the Raschig rings was prepared from Co(II) sulfate hepta-hydrate solution 3 M and the Co_3O_4 was precipitated out of the solution with KOH 3 M. The precipitate was washed with tri-distilled water and re-dispersed with concentrated acetic acid to peptize the colloidal particles of Co_3O_4 [14]. The Raschig rings were dip-coated in this Co-colloid. After drying at room temperature the impregnated RR were calcined for different times (2–10 h) and temperatures (300–500 °C) in order to optimize the catalyst spinel crystallographic structure leading to the kinetically fastest photocatalyst and concomitantly diffuse the Co-oxide into the RR. The most suitable catalyst needed calcination for 6 h at 500 °C. After calcination the loosely bound Co_3O_4 on the RR was eliminated by sonication by a procedure previously reported [15].

$Fe(OH)_3$ from a $FeCl_3$ solution was precipitated on the RR-surface and then calcined for different periods and temperatures (between 100 and 400 °C). The most suitable catalyst needed 2 h calcination times at 300 °C.

2.3. Elemental analysis of the Co-content of the Co_3O_4/Raschig rings

The elemental analysis (EA) of the Co-content on the RR before and after the photocatalytic process was carried out by atomic absorption spectrometry using a Perkin-Elmer 300S unit after digesting the Co_3O_4 on the RR surface with a solution HCl 1 M.

2.4. Irradiation procedures

The photodiscoloration/mineralization of Orange II was carried out in (a) small cylindrical photochemical reactors having each 80 mL capacity and containing 50 mL solution. Each reactor was able to accommodate 300 Raschig rings loaded with Co_3O_4. Irradiations were carried out in the cavity of a Hanau Suntest lamp (radiation flux 100 mW/cm^2 or 2×10^{16} photons/(s cm^2)) equipped with an IR filter to remove the infrared radiation and a second Pyrex filter to remove the UV radiation <310 nm. The radiant flux of the Suntest solar simulator was measured with a power-meter from YSI Corp., Colorado, USA. The short wavelength radiation ($\lambda < 310$ nm) was removed by the Pyrex wall of the reaction vessels.

The photodiscoloration/mineralization of Orange II was also carried out in cylindrical reactor in batch mode operation to assess and compare the effect of the UV-light with the simulated solar radiation mentioned above. A medium pressure mercury lamp (125 W Philips, Eindhoven, The Netherlands) was used as the light source aligned the reactor axis of the reactor having quartz walls and provided for with an external water cooling system. The main radiation was at 366 nm and other light spikes extended in the range $280\ \text{nm} < \lambda < 550$ nm. The overall radiation flux from the mercury lamp was 2.8×10^{-8} Einstein/(s cm^2) or 16.8×10^{16} photons/(s cm^2). The Orange II solution was recycled by means of a peristaltic pump at recycling rates between 200 and 400 mL/min. The total volume of Orange II solution subjected to degradation was 0.5 L. The volume treated in the reactor was of 0.23 L and a volume of 0.27 L was positioned in the tubes and the reservoir (external circuit).

2.5. Analyses of the irradiated solutions

The absorption and disappearance of Orange II solutions was followed in a Hewlett-Packard 38620 N-diode array spectrophotometer at the peak of the dye ($\lambda = 486$ nm). The total organic carbon reduction (TOC) was measured with a Shimadzu

TOC-5050A TOC analyzer. The peroxide concentration of the solutions was measured by two methods: (a) the colorimetric method developed by Hochanadel [16,17] based on the oxidation of the I^- ion and (b) a second method using Merckoquant® paper from Merck AG, Switzerland was used to confirm the results obtained by the iodometric test.

2.6. Analysis of the Co^{2+}-ions in solution during the photocatalysis

The amount Co^{2+}-ions generated in the solution during the photocatalysis was quantified by high-resolution coupled plasma spectrometry (ICPS). The samples were acidified with diluted HNO_3. The ion-beam in the plasma unit was directed through the sampling interface and then directed into the mass analyzer.

2.7. Transmission electron microscopy (TEM) and energy dispersive spectroscopy (EDS)

A field emission TEM microscope Philips CM 20 (300 kV) was used to measure the particle size of the nano-crystalline Co_3O_4 on the RR surface. The particles taken off from the Raschig ring surface and deposited on the Cu-grid covered with a C-film. Energy dispersive X-ray spectroscopy (EDS) was used to identify the deposition of Co_3O_4on the RR surface. Magnification of 10,000× up to 450,000× were used to identify the samples. The resolution normally used was of 0.5 nm.

2.8. X-ray photoelectron spectroscopy (XPS)

The XPS was performed using Mg Kα radiation of 150 W. The electron energy analyzer (Leybold EA200) was operated with a band pass energy of 75 eV in the pre-selected transmission mode. The binding energy of the spectrometer was referenced to 84.0 eV for the Au $4f_{7/2}$ signal according to the SCA A83 standard of the National Physics Laboratory [18]. The evaluation of the binding energies of the embedded Co_3O_4 was carried out following standard procedures. A reproducibility of ±5% was attained in the XPS measurements. With an ADS100 set it was possible to evaluate the XPS data by subtraction of the X-ray satellites applying the background correction according to Shirley [19]. The presence of electrostatic charging effects was controlled by measurements including charge compensation by changing the electrostatic potential at the aperture site of the electron energy analyzer.

2.9. Confocal microscopy

Confocal microscopy is used increasingly for the investigation of films having thickness in the micron range. The reflection optics makes possible a resolution and depth of focus beyond the thickness possible in an atomic force microscope. The equipment is made of a camera, a control unit and a monitor and provides a high-resolution image generation (Nikon Optiphoto Co., Tokyo, Japan). The system is designed to detect the optical signals at any point of the image. In a confocal microscope, the sample surface is scanned by He–Ne laser (6 mW). The microscope is provided for with an acousto-optic modulator which directs the laser beam as a function of the modulation applied on the crystal. The only signals detected are the ones that pass through the pin-hole behind the photo-detector over the whole surface area of the image. The reflected light by the sample comes back and after being detected it is registered and stored. Confocal microscopy uses two lenses to focus the target image in a way that the plane due to the first lens overlaps with the plane of the second lens. This allows to monitor the detailed topography of the sample topmost layers having a high irregular profile.

3. Results and discussion

3.1. Suntest simulated daylight irradiation photodiscoloration of Orange II in a batch reactor

Fig. 1(A and B) shows the effect of the calcination temperature and calcination times of Co_3O_4/RR on the photodiscoloration of Orange II in the acidic and basic pH range at with values pH 2.9 and 8.0, respectively. Fig. 1(A) shows the remarkable accelerating effect of the photocatalyst addition during the photodiscoloration of Orange II. It can be seen that at an initial of pH 2.9 (Fig. 1(A)) and 8.0 (Fig. 1(B)), the Co_3O_4/RR

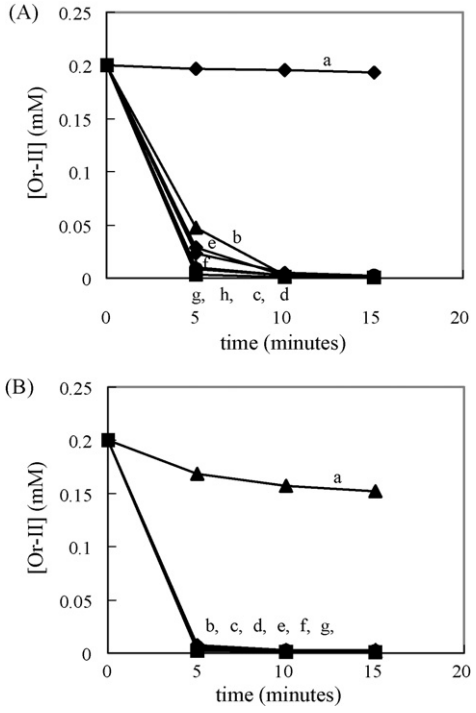

Fig. 1. (A) Effect of calcination temperature and time on the photdiscoloration of Orange II at initial pH 2.9. (a) 0.2 mM Or-II + 2 mM oxone, (b) a + Co_3O_4/RR (300 °C–2 h, (c) a + Co_3O_4/RR (300 °C–6 h), (d) a + Co_3O_4/RR (300 °C–10 h), (e) a + Co_3O_4/RR (400 °C–6 h), (f) a + Co_3O_4/RR (400 °C–10 h), (g) a + Co_3O_4/RR (500 °C–6 h), (h) a + Co_3O_4/RR (500 °C–10 h). (B) Effect of calcination temperature and time on the photodiscoloration of Orange II at initial pH 8.0. (a) 0.2 mM Or-II + 2 mM oxone, (b) a + Co_3O_4/RR (300 °C–2h), (c) a + Co_3O_4/RR (300 °C–6 h), (d) a + Co_3O_4/RR (300 °C–10 h), (e) a + Co_3O_4/RR (400 °C–6 h), (f) a + Co_3O_4/RR (400 °C–10 h), (g) a + Co_3O_4/RR (500 °C–6 h).

calcined at 300 °C for 6 and 10 h showed the best results. In all cases, the final pH observed after photodiscoloration was ~2.6 due to the acidification caused by the added oxone. The accelerated Orange II discoloration was observed to occur within 5 min. By elemental analysis (EA) the Co-content at times zero and 5 min was determined to be 64.8% and 65.2%, respectively. These values are in the experimental error of the determination implying that no loss of Co occurred during the photocatalytic process.

The results obtained for the discoloration of Orange II with Fe_2O_3/RR were similar to the results reported in Figs. 1–3 for the Co_3O_4/RR catalyst. This is why we do not explicitly describe the results in the present study.

3.2. *Effect of the recirculation rate, Orange II concentration and solution pH on the dye discoloration/mineralization in a reactor in batch mode operation*

After preliminary experiments to optimize the performance of the Co_3O_4/RR catalyst in a batch reactor we moved to photoreactor experiments in batch mode operation. This allows the recycling of Orange II using larger volumes. Fig. 2 shows the effects of the recirculation rate on the discoloration (A) and mineralization (B) of Orange II with oxone mediated by Co_3O_4/RR under UV light. Fig. 2(A) shows that the effect of oxone is to accelerate the photodiscoloration of Orange II (traces a and b). In the presence of Co_3O_4/RR, the most suitable discoloration/mineralization is observed in trace (c) when the circulation rate was fixed at 400 mL/min. This recirculation rate increased the amount of light per unit time of the solution been irradiated in the reactor and allowed a more appropriate mixing of the reactants during the process [20]. Trace (d) shows the effect of a recirculation rate of 200 mL/min allowing a longer residence time in the dark part of the reactor (tubes and reservoir) with a consequent decrease in the observed discoloration/mineralization rate.

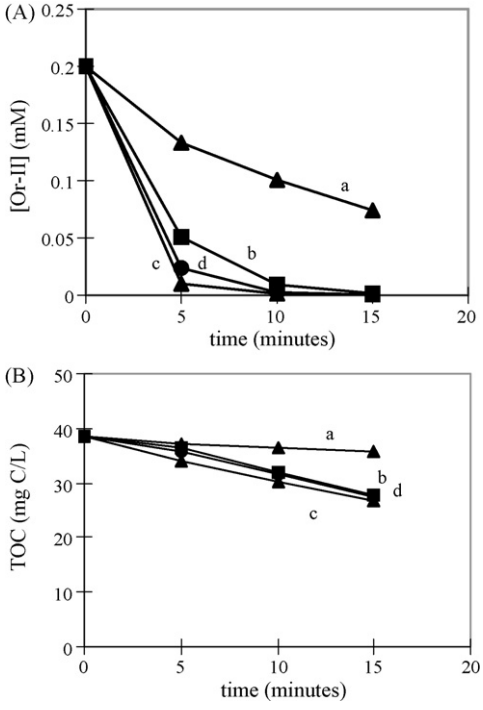

Fig. 2. Effects of the reactor recirculation rate on Orange II discoloration (A) and mineralization (B) by oxone mediated by Co_3O_4/RR under UV-light. (a) 0.2 mM Or-II + 400 mL/min, (b) 0.2 mM Or-II + 2 mM oxone + 400 mL/min, (c) 0.2 mM Or-II + 2 mM oxone + Co_3O_4/RR + 400 mL/min, (d) 0.2 mM Or-II + 2 mM oxone + Co_3O_4/RR + 200 mL/min.

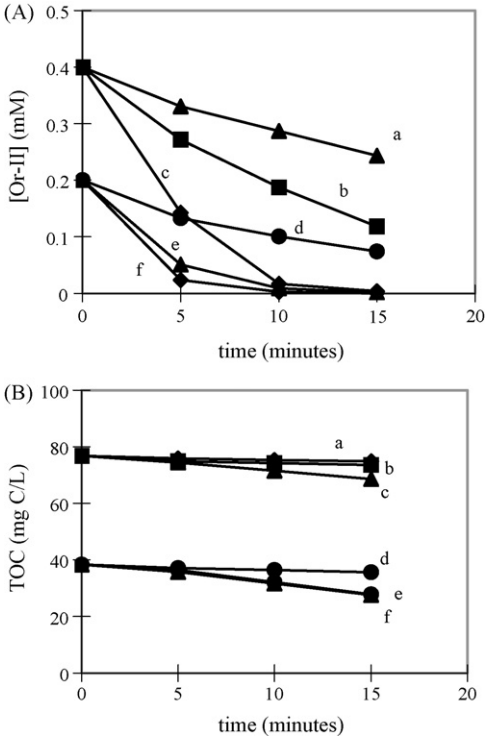

Fig. 3. Photodiscoloration (A)/mineralization (B) of Orange II by oxone mediated with Co_3O_4/RR under UV light, recirculation rate = 400 mL/min. (a) 0.4 mM Or-II, (b) 0.4 mM Or-II + 2 mM oxone, (c) 0.4 mM Or-II + 2 mM oxone + Co_3O_4/RR, (d) 0.2 mM Or-II, (e) 0.2 mM Or-II + 2 mM oxone, (f) 0.2 mM Or-II + 2 mM oxone + Co_3O_4/RR.

The variation of the oxone concentration on the photodiscoloration/mineralization of Orange II under the experimental conditions used in Fig. 2(A)/(B) was negligible. The photodiscoloration was completed always within 10 min.

Fig. 3(A)/(B) shows the discoloration/mineralization of solutions with different Orange II concentrations under the same conditions as used in Fig. 2. The beneficial effect of oxone alone and of oxone in the presence of Co_3O_4/RR is readily seen in the two Orange II solutions with initial Orange II concentration in Fig. 3 (see caption to figure). That the dye discoloration/mineralization is a diffusion controlled process is readily seen in Fig. 3. Longer times were observed in Fig. 3(A) for the discoloration of a higher concentration of Orange II (0.4 mM).

When the initial pH was varied from 2.9 to 10.8, the discoloration kinetics in practice did not vary. Since the Co-ions precipitate out of the solution at pH values between 7 and 8, the catalysis is mainly due to the fixed Co_3O_4 clusters on the RR and

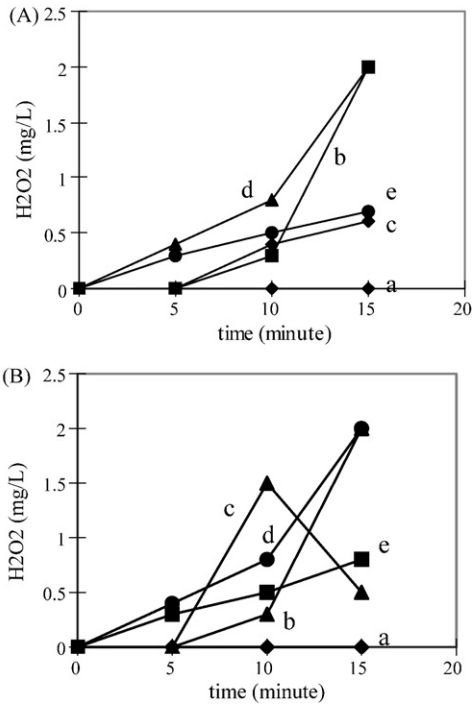

Fig. 4. (A) Generation of H_2O_2 by oxone mediated with Co_3O_4/RR under UV light, recirculation rate 400 mL/min. (a) 0.2 mM Or-II initial pH 6, (b) 0.2 mM Or-II + 2 mM oxone, initial pH 2.9, (c) b + Co_3O_4/RR, initial pH 2.9, (d) 0.2 mM Or-II + 2 mM oxone, initial pH 10.8, (e) d + Co_3O_4/RR, initial pH 10.8. (B). Generation of H_2O_2 by oxone mediated with Fe_2O_3/RR under UV light, recirculation rate = 400 mL/min. (a) 0.2 mM Or-II, initial pH 6.0, (b) 0.2 mM Or-II + 2 mM oxone, initial pH 2.9, (c) b + Fe_2O_3/RR (initial pH 2.9, (d) 0.2 mM Or-II + 2 mM oxone, initial pH 10.0, (e) d + Fe_2O_3/RR, initial pH 10.8.

not due to the Co-ions free in solution in acidic range. Further information about this point is found in Section 3.4 below when discussing the results obtained by coupled plasma spectrometry (ICPS).

3.3. Generation of H_2O_2 during the discoloration of Orange II mediated by Co_3O_4/RR and Fe_2O_3/RR catalysts

Fig. 4(A) shows the generation of H_2O_2 during the discoloration of Orange II by oxone in the presence of Co_3O_4/RR under UV light irradiation. Trace a shows that in the absence of oxone the generation of H_2O_2 under UV-light is not possible, but the addition of oxone (traces b and c) lead to the generation of H_2O_2 in acidic solutions. In basic solutions, the generation of H_2O_2 is observed to be more effective in Fig. 4 on Co_3O_4/RR than when oxone was used alone confirming the beneficial role of the Co_3O_4 active sites on the Raschig rings as responsible for the oxone decomposition. The generation of H_2O_2 was possible as long as Orange II remained in solution and stopped after 15 min irradiation. The degradation intermediates were seen not to be conducive to the generation of H_2O_2. The mechanism of H_2O_2 generation presented in Fig. 4 will be discussed in Section 3.5 below.

Fig. 4(B) shows the generation of H_2O_2 during the discoloration of Orange II by oxone in the presence of Fe_2O_3/RR under UV-light irradiation. The results obtained are similar to the ones reported in Fig. 4(A) with one exception. Trace (c) shows a notable decrease in the generation of H_2O_2 after 10 min. This is due to the known dissolution of Fe_2O_3 in the acidic pH-range. This also confirms the higher stability of the Co_3O_4/RR catalyst and its choice as the focus of the attention in this study.

Table 1
Free Co^{2+} (mg/L) in solution in the system (0.2 mM Orange II + 2 mM oxone + Co_3O_4/RR) irradiated under Suntest light (100 mW/cm^2)

T–t^*	System pH	5 min	10 min	15 min
300 °C–6 h	2.9	1.06	2.24	1.65
400 °C–6 h	8.0	0.48	0.78	0.57
500 °C–10 h	8.0	0.38	1.61	1.38

T–t^*: calcination temperature and time for Co_3O_4/RR respectively.

3.4. Determination of Co^{2+} during the discoloration of Orange II by ICPS and implications for the natural cycle

As determined by induced coupled plasma spectrometry (ICPS), Co^{2+}-ions are produced during the photodiscoloration of Orange II as carried out in Fig. 1. This is shown next in Table 1. This suggests the involvement of Co-ions in homogeneous processes contributing to the degradation of Orange II on the Co_3O_4/RR and is noted in the overall scheme of reaction in Section 3.5.

Table 1 shows the increase of Co-ions as the Orange II progresses up to 10 min and then a decrease. For runs at 300 °C (Table 1), runs zero, 2, 4 and 6 min indicated Co^{2+}-ions with ppm concentrations of 0.05, 0.53, 0.46 and 1.0, respectively. Levels of cobalt below 1–2 ppm have been reported not to be hazardous to animal health in agricultural waters [21].

The Co^{2+}-ions in solution seems to get re-oxidized by the oxone present and return to the Co_3O_4/RR surface due to: (a) the predominance of the photocatalyst mass present in the solution and (b) the re-oxidation of Co^{2+}-ions due to the oxone present in the oxidative media able to precipitate back of Co^{2+}-ions into the crystallographic structure of Co^{3+} in the Co_3O_4. This mechanism of ion-release and adsorption onto a surface is one of the common routes by which nature mineralize refractory materials in the natural cycle. It is a well-known mechanism for soil and ground water remediation [1,22]. This mechanism suggests that after Orange II discoloration, the Co-ions in solution go back to the Co_3O_4/RR surface and are ready to participate in a new degradation cycle [23].

3.5. Suggested mechanism of reaction

Figs. 1–4 show the effect of light being absorbed by Orange II producing the charge transfer with Co_3O_4/RR transfer noted in Eq. (1) below leading to the unstable cation Orange II$^{\bullet+}$ [10–13]. Eqs. (2)–(6) outline the intervention of the oxone (HSO_5^-) and related highly oxidative radicals produced in aqueous solution by oxone in the presence of O_2. Eq. (7) relate to the Orange II mineralization as reported above in

Figs. 1–3. Finally, the peroxide formation due to the interaction of the radical(s) $R^{\bullet}$ with O_2 leading to peroxides is noted in Eq. (8)

$$\text{Orange II} + \text{RR/Co}_3\text{O}_4 + h\nu \rightarrow [\text{Orange II}^* + \text{RR/Co}_3\text{O}_4] \rightarrow \text{Orange II}^{\bullet+} + \text{RR/Co}_3\text{O}_4\text{e-}_{cb}\ (\text{or } \text{Co}^{2+}) \quad (1)$$

$$\text{Orange II}^* + \text{HSO}_5^- \text{ (oxone in net sense)} \rightarrow \text{Orange II}^{\bullet+} + (\text{HO}^- + \text{SO}_4^{\bullet-}) \quad (2)$$

$$\text{RR/Co}_3\text{O}_4\ \text{e-}_{cb}\ (\text{or } \text{Co}^{2+}) + \text{HSO}_5^- \rightarrow \text{Co}^{3+} + \text{SO}_4^{2-} + \text{HO}^- \quad (3)$$

$$\text{Orange II}^{\bullet+} + \text{HSO}_5^- \rightarrow \text{Organics/radicals}\ (\text{R}^{\bullet}) + (\text{HO}^- + \text{SO}_4^{\bullet-}) \quad (4)$$

$$\text{Organics/R}^{\bullet} + \text{Co}^{3+}/\text{Co}^{2+}/\text{HO}^-/\text{SO}_4^{\bullet-} \rightarrow \text{Long-lived intermediates.} \quad (5)$$

$$\text{HSO}_5^- + (\text{OH or } \text{SO}_4^{\bullet-}) \rightarrow \text{SO}_5^{\bullet-} + (\text{HO}^- \text{ or } \text{SO}_4^{2-} + \text{H}^+ \quad (6)$$

$$\text{R}^{\bullet} + \text{HSO}_5^-/\text{O}_2 \rightarrow \text{Organics} \rightarrow \text{CO}_2 + \text{H}_2\text{O} + \text{SO}_4^- \quad (7)$$

$$\text{R}^{\bullet} + \text{O}_2 \rightarrow \text{ROO}^{\bullet} \quad (8)$$

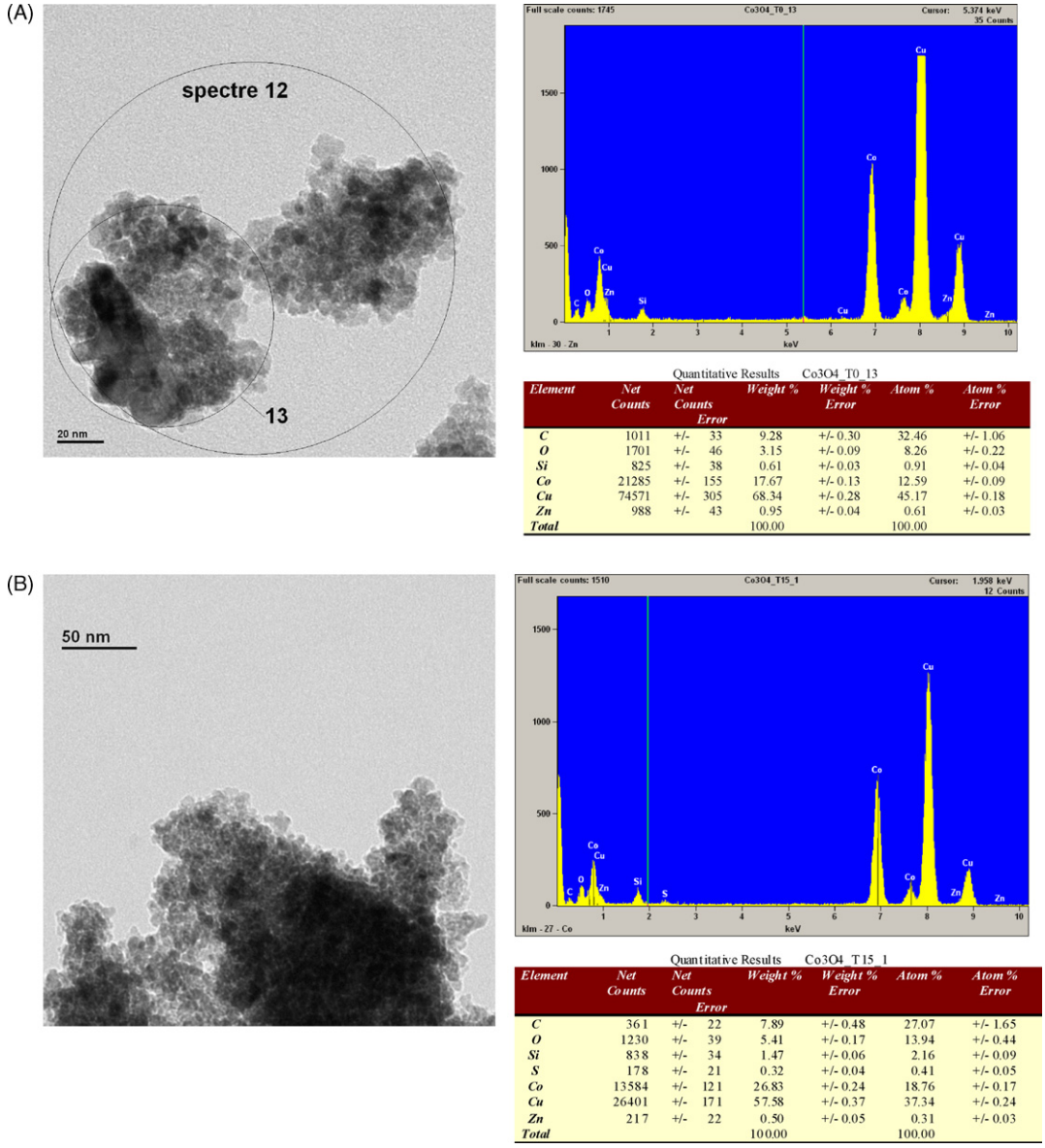

Fig. 5. (A) Transmission electron microscopy of Co_3O_4/RR at time zero showing the Co-oxide particles and the EDS spectra. For more details see text. (B) Transmission electron microscopy of Co_3O_4/RR rings after 15 min photocatalysis showing the Co-oxide particles and the EDS spectra. For more details see text.

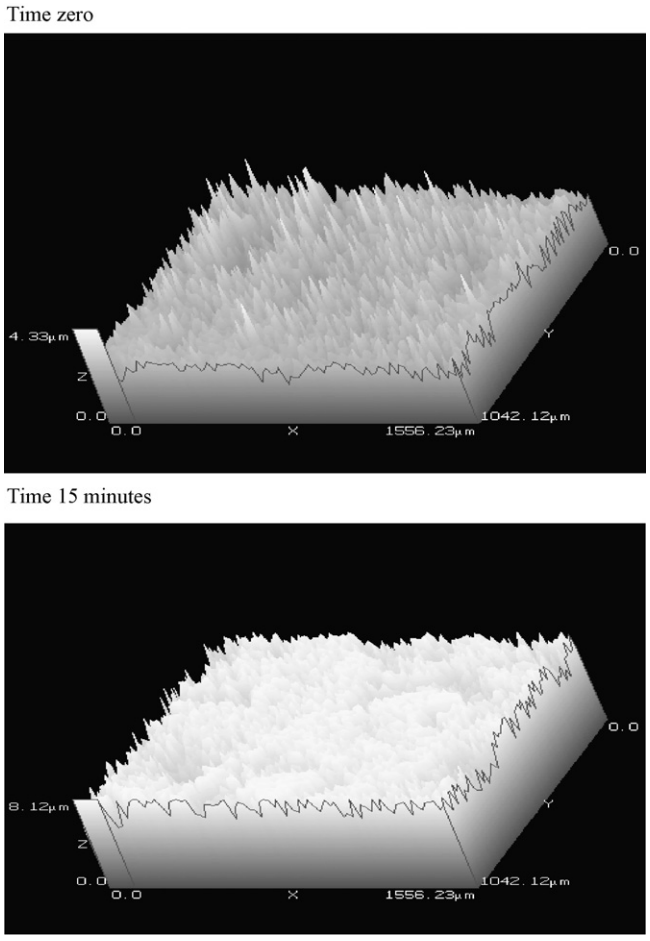

Fig. 6. Confocal microscopy of the surface of Co_3O_4/RR at times zero and after the 15 min photo-reactor UV-treatment of Orange II in the presence of oxone. For other experimental details see text.

3.6. Transmission electron microscopy (TEM) and energy dispersive spectroscopy (EDS)

Fig. 5(A and B) shows the TEM of Co_3O_4/RR samples at zero and 15 min reaction. Co-particles with size distribution 2–10 nm were counted in both cases and no variation in the Co-particle size or size distribution was observed after the photocatalysis. The relative atom enrichment of Co at time zero of 12.59% increases to 18.76% after 15 min reaction. The surface of the catalyst has been cleaned in the process showing less C-content (27.07% compared to 32.46%) allowing the surface Co-enrichment. The Si and Zn detected by EDS are impurities introduced by the precursor compounds during the preparation of the samples. The low amount of S detected after the photocatalysis stems from the Orange II degradation intermediates in solution that are subsequently adsorbed on the catalyst surface.

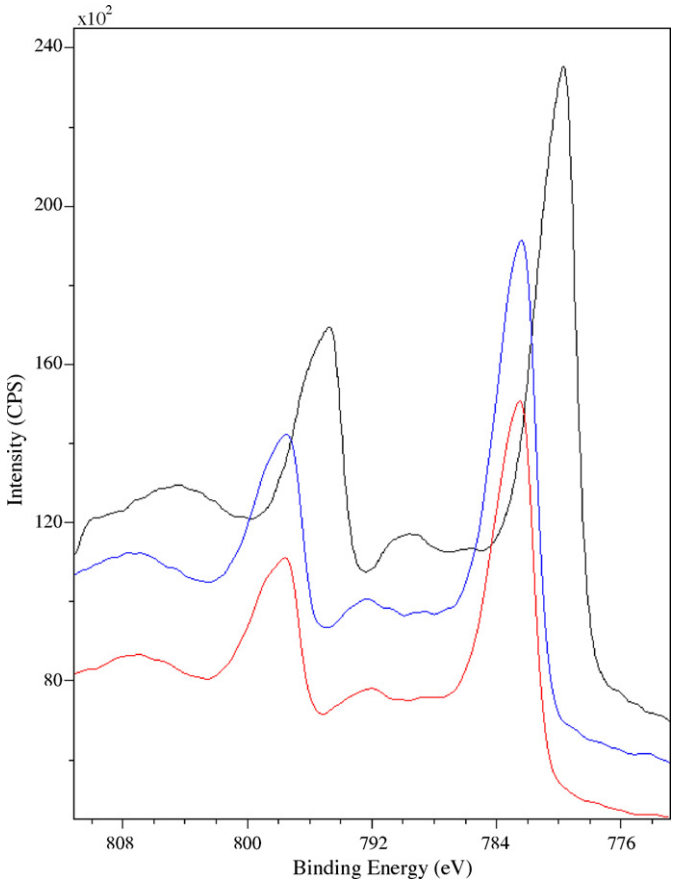

Fig. 7. XPS of Co from the Co_3O_4 during the photocatalysis of Orange II.

3.7. Confocal microscopy studies of Co_3O_4/RR samples

Confocal microscopy has been selected to analyze the irregular profile of the surfaces showing valleys and peaks with dimensions in the micron range (Fig. 6) since the resolution of this thickness was not possible with atomic force microscopy (AFM). Fig. 6 shows at time zero a peak height of 4.33 μm for the Co_3O_4 deposit coating on RR. The settings of the confocal microscope oscillated between 38.80 and 43.13 μm. The image disappeared on the highest and lowest levels of the film setting this difference for the peak heights and valleys. The retention of the Co_3O_4 particles depends on the RR-glass rugosity. This determines the small sizes observed for the Co_3O_4 islands entrapped on the RR.

Fig. 6 shows that after 15 min the peak height increased up to 8.12 μm with concomitant increase in the crevices and porosity. This reveals an interaction between Co_3O_4 layers with the oxone and Orange II present in solution under UV-irradiation. Th distribution of the peaks and valleys changed after 15 min

Table 2
Surface atomic concentrations in % of the most abundant elements on Co_3O_4 Raschig rings

Sample	C	O	Co	N	O/C × 10	Co/O × 10	C/Co × 10
On glass Co_3O_4, $t = 0$	20.14	50.66	28.88		25.2	5.7	7.0
On glass Co_3O_4, $t = 10$ min	27.17	45.85	26.63	1.35	16.9	5.8	10.2
On glass Co_3O_4, $t = 15$ min	23.52	49.07	27.14	0.26	20.9	5.5	8.7

reaction compared the ones found at time zero. The distance between the peaks and the valleys of 8.12 μm was observed to increase with respect to the time zero values (4.33 μm). Higher peaks after the photocatalysis means less densely packed Co_3O_4 particles compared to time zero.

3.8. X-ray photoelectron spectroscopy (XPS) of the Co_3O_4/RR samples

The surface atomic concentration for C, O, Co and N are shown in Table 2.

From Table 2 it is readily seen that the amount C and O and Co remains almost constant during the photocatalysis up to 15 min. The variations observed for their atomic concentration are in the experimental range of error the XPS measurements. The N-concentration of 1.35% shows that the highest amount of adsorbed Orange II takes place after 10 min. It is interesting that at time zero, Orange II is not adsorbed on the Co_3O_4 Raschig rings. The quick decomposition of N-species as seen by the low surface concentration of N at 15 min, once more indicates the efficiency of the photocatalyst decomposition not allowing the accumulation of residues during the decomposition of Orange II. There is no accumulation of intermediates on surface of catalyst with time.

The XPS spectra of the recorded Co2p, O1s, C1s and N1s lines for the samples of Orange II irradiated as in Fig. 1 on Co_3O_4 Raschig rings after different reaction times are presented in Figs. 7–10. Fig. 7 shows a striking observation: the very large shift of Co2p3/2 line from position at 779.6 eV at time 0–782.2 eV at reaction times 10 and 15 min. This indicates a strong reduction of electron density on cobalt atoms of the catalyst and support strong oxidation properties of this oxide [18]. By the analysis of the thinnest outermost layer after time zero it was found that the first atomic surface layers of cobalt for the peak Co2p3/2 (around 1 nm) were already strongly reduced at 781.1 eV while the thick surface layer (3–4 nm) showed a Co2p3/2 peak at 779.6 eV. This indicates that even without any radiation the most surface cobalt atoms are strong electron donors to first adsorbed surface species.

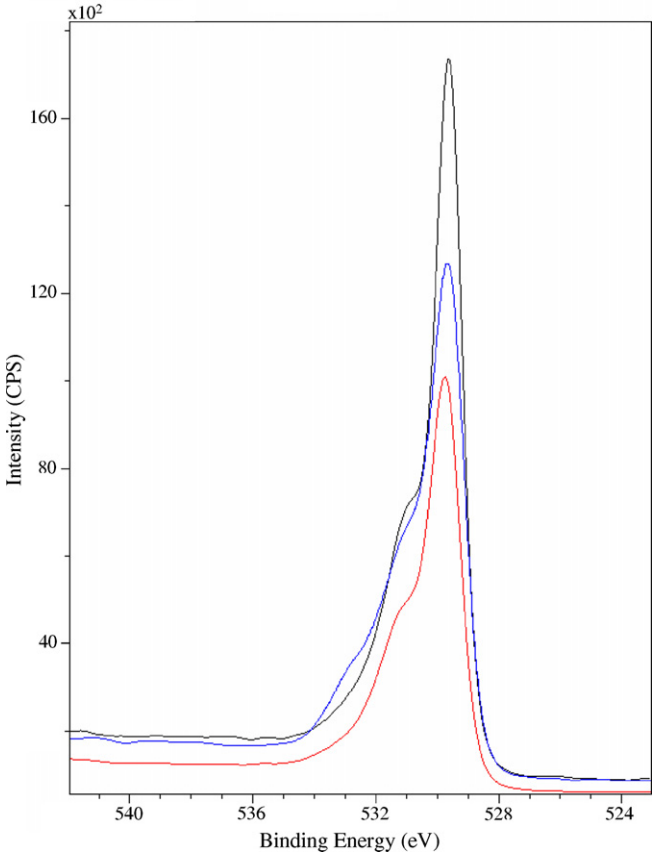

Fig. 8. XPS of O from the Co_3O_4 during the photocatalysis of Orange II.

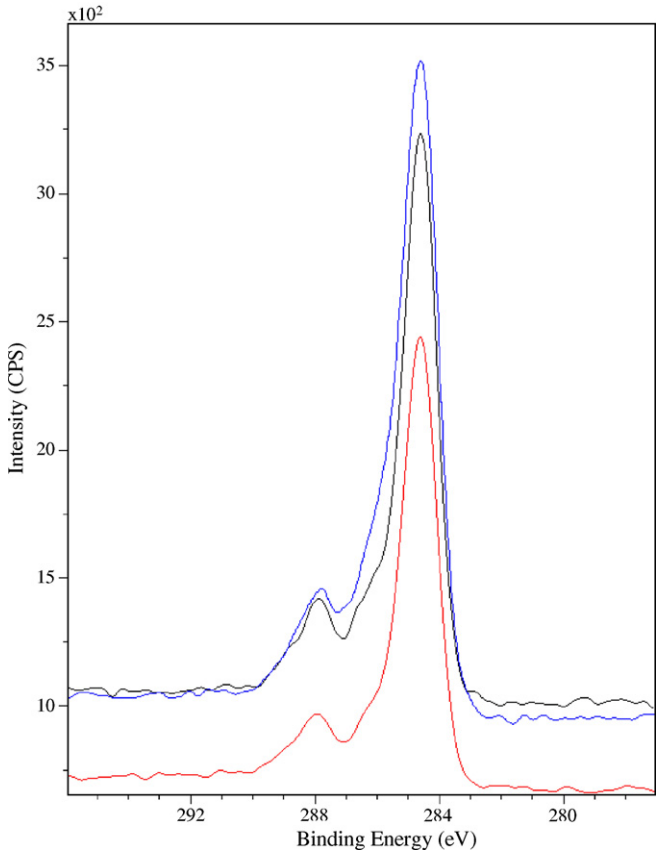

Fig. 9. XPS of N from the Co_3O_4 during the photocatalysis of Orange II.

The highest amount of adsorbed Orange II and intermediate species take place after 10 min. The lower intensity of Co2p (Fig. 7) and O1s (Fig. 8) lines and the concomitant highest intensities of the C1s (Fig. 9) and N1s (Fig. 10) lines provide the evidence for this observation. After 15 min of reaction there is a strong removal of intermediates from the catalyst surface (Table 2, C/Co ratio). The produced intermediates contain significant amount of C–O and COOH molecular groups [18] (see Fig. 9). It is also worth to note that at time zero Orange II is not the major adsorbed surface species like would be expected. The signal from N1s line is lower (spectra not shown in Fig. 10) than the sensitivity of the XPS method (1% of a monolayer). This observation suggests that the Orange II molecules after adsorption undergo immediately catalytic decomposition (see Table 2, time zero for N-values).

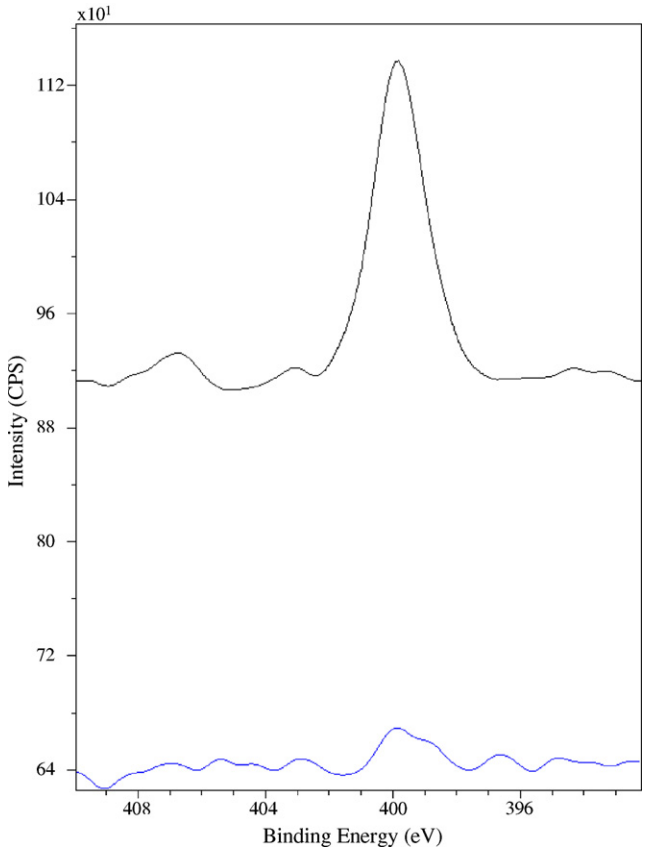

Fig. 10. XPS of C from the Co_3O_4 during the photocatalysis of Orange II.

4. Conclusion

The UV light induced discoloration/mineralization of Orange II using oxone as the oxidant and Co_3O_4/RR as the photocatalyst under UV light was investigated. The parameters controlling the Co_3O_4/RR synthesis were explored in detail and related to the nature and concentration of the Co-species employed, the pH of the precursor solution and the calcination time and temperature. The solution parameters evaluated during the optimization of the discoloration kinetics were: the dye concentration, the reactor recirculation rate, the oxone concentration and the solution pH. It is suggested that the fast discoloration of Orange II occurring within 5 min was mainly due to: (a) the large contact area provided by the Raschig rings inside the reactor and (b) the small size of the Co_3O_4 clusters (2–10 nm) attached to these RR. Insight is provided for the chemistry of the oxone involved in Orange II degradation mediated by Co_3O_4/RR.

The low amount of Co^{2+}-ions entering the solution remained under the limit allowed for Co-ions in agricultural drinking waters. The catalyst investigated in this study is of low cost, easy to prepare and to handle. It was shown that it sustains long-term operation. This points out favorably to the potential practical application of this catalyst on a broader scale.

Acknowledgment

We thank COST Action 540 "Photocatalytic technologies and novel nano-surface materials, critical issues" for their support (Bern, Switzerland).

References

[1] Th. Oppenlaender, Photochemical Purification of Water and Air, Wiley-VCH, Weinheim, Germany, 2003.
[2] A. Mills, S.L. Hunte, J. Photochem. Photobiol. A 108 (1997) 1–17.
[3] A. Fujishima, T. Rao, D. Tryk, J. Photochem. Photobiol. C 1 (2000) 1–21.
[4] M.R. Hoffmann, S.T. Martin, W. Choi, D.W. Bahnemann, Chem. Rev. 95 (1995) 69.
[5] A. Mills, S.-K. Lee, J. Photochem. Photobiol. A 152 (2002) 233–247.
[6] D.F. Ollis, H. Al-Ekabi, Photocatalytic Purification and Treatment of Water and Air, Elsevier Pub. Co., Amsterdam, 1993.
[7] P. Raja, M. Bensimon, A. Kulik, R. Foschia, D. Laub, P. Albers, R. Renganathan, J. Kiwi, J. Mol. Catal. A 237 (2005) 215–223.
[8] P. Raja, J. Bandara, P. Giordano, J. Kiwi, Ind. Eng. Chem. Res. 44 (2005) 8959–8967.
[9] J. Fernandez, J. Kiwi, J. Baeza, J. Freer, C. Lizama, H.D. Mansilla, Appl. Catal. B 48 (2004) 205–211.
[10] G. Anipsitakis, D. Dionysiou, Environ. Sci. Technol. 54 (2004) 155–163.
[11] J. Kim, J. Edwards, Inorg. Chim. Acta 235 (1995) 9–21.
[12] J. Fernandez, V. Nadtochenko, J. Kiwi, Chem. Commun. (2003) 2382–2383.
[13] J. Fernandez, P. Maruthamuthu, A. Renken, J. Kiwi, Appl. Catal. B 49 (2004) 207–215.
[14] F. Svegl, B. Orel, I. Grabec-Svegl, V. Kaucic, Electrochim. Acta 45 (2000) 4359–4371.
[15] M. Dhananjeyan, E. Mielczarski, K. Thampi, Ph. Buffat, M. Bensimon, A. Kulik, J. Mielczarski, J. Kiwi, J. Phys. Chem. B 105 (2001) 12046–12055.
[16] C. Hochanadel, J. Phys. Chem. 56 (1952) 587–594.
[17] J. Kiwi, M. Graetzel, Chem. Phys. Lett. 78 (1981) 241–245.
[18] D. Briggs, M. Sheah, Auger and X-ray Photoelectron Spectroscopy, vol. 1, second ed., John Wiley, Chichester, UK, 1990.
[19] A. Shirley, Phys. Rev. 179 B5 (1972) 4709–4716.
[20] E. Balanosky, F. Herrera, A. Lopez, J. Kiwi, Water Res. 43 (2000) 582–596.
[21] C. Anzec, Z. Armcan, Australian and New Zealand Guidelines for Fresh and Marine Water Quality, vol. 3, chapter 9 from the Agriculture and Resource Management Council of Australia, 1994.
[22] G. Helz, R. Zepp, D. Crosby, Aquatic and Surface Chemistry, Lewis Pub. Co., Boca Raton, FL, 1994.
[23] J. Bandara, J. Kiwi, New J. Chem. 23 (1999) 717–724.